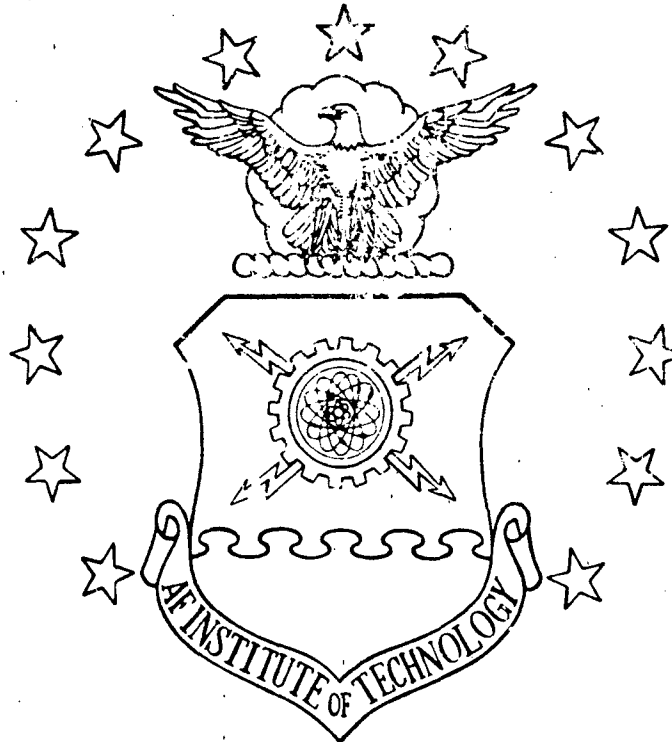


AD-A151 940



Reproduced From
Best Available Copy

AUTOFOCUS MOTION COMPENSATION FOR SYNTHETIC APERTURE
RADAR AND ITS COMPATIBILITY WITH STRAPDOWN INERTIAL
NAVIGATION SENSORS ON HIGHLY MANEUVERABLE AIRCRAFT

THESIS

Henry D. Baird, Jr.
Captain, USAF

AFIT/GA/ENG/84D-1

DTIC FILE COPY

DISTRIBUTION STATEMENT A
Approved for public release
Distribution Unlimited

DTIC
ELECTE
MAR 29 1985
S
B

DEPARTMENT OF THE AIR FORCE
AIR UNIVERSITY
AIR FORCE INSTITUTE OF TECHNOLOGY

Wright-Patterson Air Force Base, Ohio

20000807032 85 03 13 059

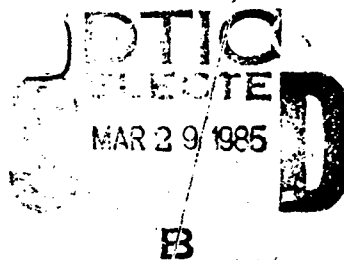
AFIT/GA/ENG/84D-1

**AUTOFOCUS MOTION COMPENSATION FOR SYNTHETIC APERTURE
RADAR AND ITS COMPATIBILITY WITH STRAPDOWN INERTIAL
NAVIGATION SENSORS ON HIGHLY MANEUVERABLE AIRCRAFT**

THESIS

Henry D. Baird, Jr.
Captain, USAF

AFIT/GA/ENG/84D-1



Approved for public release; distribution unlimited

AFIT/GA/ENG/84D-1

AUTOFOCUS MOTION COMPENSATION FOR SYNTHETIC APERTURE RADAR
AND ITS COMPATIBILITY WITH STRAPDOWN INERTIAL NAVIGATION
SENSORS ON HIGHLY MANEUVERABLE AIRCRAFT

THESIS

Presented to the Faculty of the School of Engineering
of the Air Force Institute of Technology

Air University

In Partial Fulfillment of the
Requirements for the Degree of

Master of Science in Astronautical Engineering

Henry D. Baird, Jr., B.S.

Captain, USAF

December 1984

Approved for public release; distribution unlimited

Preface

This study undertakes to determine the feasibility of using present day strapdown inertial navigation systems to motion compensate synthetic aperture radars, and in particular, motion compensation using the autofocus technique. It is important to understand that the autofocus technique is only one of many methods being investigated in the field as the best means to motion compensate a highly accurate radar detection system. It would be beyond the capabilities of myself and that of a thesis to undertake a thorough study of all the motion compensation techniques available. I have attempted to make the reader understand this particular form of motion compensation and its very real possibilities as the most capable for highly dynamic aircraft. The ability to use synthetic aperture radar in extremely maneuverable aircraft is only now becoming possible due to very small but highly capable onboard digital computers. The combination of these computers and the robustness of the strapdown inertial systems and synthetic aperture radars promise to make the aircraft of tomorrow a formidable weapon system.

It was very interesting to me in my capacity as an F-111 Weapon Systems Officer to investigate the possibilities inherent in synthetic aperture radar and strapdown inertial navigation systems. Their low life-cycle-cost and maintainability seem to make it imperative that more research is undertaken in this field.

I would like to take this opportunity to thank those involved in my quest for knowledge at AFIT. My thesis advisor, Dr. Slouris, was extremely helpful and always ready to steer me in the right direction if I happened to stray from the straight and narrow. Lt Col Watt, my faculty advisor, was very helpful when I thought the going was getting too tough and encouraged me to keep at it just a little longer. And finally, my wife and children, who always kept things in perspective and made the experience worthwhile.

Table of Contents

	Page
Preface	ii
List of Figures	v
List of Tables	vi
Abstract	vii
I. Introduction	1
Background	1
Problem	1
Scope	2
Development	2
II. Real and Synthetic Radar	4
Resolution Cell Size	5
X-Direction Resolution	5
Y-Direction Resolution	8
III. SAR Focusing and Aperture Weighting	15
IV. SAR Phase Errors and Image Quality	18
Low Frequency Errors	18
High Frequency Errors	20
Summary	22
V. INS Characteristics and Capabilities	24
Unaided INS	24
Aided INS	28
VI. SAR Motion Compensation Requirements	31
LOS Acceleration Measurement Error	31
LOS Centripetal Acceleration Error	34

List of Figures

2.1	Geometry of a Real Array Imaging Radar	5
2.2	Radar Range Gates	6
2.3	Resolution in the X-Direction	6
2.4	Resolution of Two Points a Distance d Apart	12
2.5	Actual and Theoretical Y-Direction Resolution	14
3.1	Parabolic Reflector	15
3.2	Uniform Phase Aircraft Flight Profile	16
3.3	Radiation Pattern for Uniformly Illuminated Arrays	17
4.1	Types of SAR Phase Errors	18
4.2	Effect of Quadratic Phase Error on Resolution and Gain	20
4.3	Side Lobe Energy Due to High Frequency Phase Errors	21
4.4	Visual Effects of Poor QPE, PSLR, and ISLR	22
5.1	Typical INS Navigation Errors	25
6.1	Aircraft Closure Geometry	34
7.1	Autofocus Interface	37
7.2	Subarray Linear Phases with Opposite Slopes Caused by Quadratic Phase on Full Array	38
7.3	Block Diagram of Map Drift Autofocus Algorithm	39
7.4	Performance Envelope Sensitivity to Various Levels of Motion Compensation Capability	41
7.5	Aircraft Maneuver Effects on SAR Range-Squint Angle Focus Regions	42

List of Tables

Table	Page
2.1 Resolution Cell Size for Various Objects	5
2.2 Representative Integration Times and Aperture Lengths	14
5.1 Representative INS Position Errors	28
5.2 Projected Aided INS Performance	29
5.3 Acceleration Measurement Error Budget	30
6.1 LOS Acceleration Accuracy Requirements vs Squint Angle	33
6.2 LOS Acceleration Accuracy Requirements vs Aircraft Speed	33
6.3 Velocity Accuracy Requirements	36

7
D
2

AUTOFOCUS MOTION COMPENSATION FOR SYNTHETIC APERTURE RADAR
AND ITS COMPATIBILITY WITH STRAPDOWN INERTIAL NAVIGATION
SENSORS ON HIGHLY MANEUVERABLE AIRCRAFT

I. Introduction

Background

As modern military aircraft have become more sophisticated, and more expensive, their ability to pinpoint targets on the ground and strike those targets with weapons equally sophisticated and expensive has lagged behind. In the past, gimballed Inertial Navigation Systems (INS) have provided precise autonomous navigation and position information for military aircraft. The mechanical complexity and penalties of gimballed systems such as maintainability, reliability, and Life-Cycle-Cost (LCC) limit their application. These systems cannot realize the low cost and reliability of strapdown inertial systems utilizing ring laser gyroscopes or tuned gyroscopes such as the SPN-GEANS or N-73. Strapdown Inertial Navigation Systems utilizing either tuned gyroscopes or ring laser gyroscopes and advanced accelerometers may alleviate the poor maintenance record of inertial platforms which have plagued the advanced aircraft of today. These strapdown inertial systems must significantly reduce their LCC without sacrificing performance and accuracy. It is felt that with the availability of small high-speed digital minicomputers the strapdown INS has finally become an effective system. Also, strapdown inertial navigation systems have become nearly as accurate as their predecessors, and as this study will show, capable of handling the motion compensation tasks of modern radar applications.

Problem

Modern military aircraft's ability to navigate using their onboard radar to update the

inertial navigation system has been held back by the lack of high definition information coming from the radar system. Although the increasing sophistication of modern military aircraft has made it possible for them to handle much more difficult tasks and an ever expanding role in the Air Order of Battle, their ability to seek out and identify targets more accurately has not kept up with other more technologically advanced areas of aviation. Synthetic Aperture Radar (SAR) may be able to provide a much better picture of the terrain with which to update the onboard navigation systems. Synthetic Aperture Radar's promise in the area of enhanced resolution of the radar picture may be held back only by its lack of highly accurate information from the inertial navigation system with which to allow motion compensation. The combination of improved navigation and target tracking systems promise to make the aircraft of tomorrow far superior to anything now flying.

Scope

It is the intention of this study to show that the motion compensation requirements of synthetic aperture radars aboard these modern military aircraft can be met by strapdown inertial navigation systems that are available at present. Fundamental to motion compensation and high resolution Synthetic Aperture Radar is the concept of focusing. In particular, the autofocus technique of motion compensation is explored. The autofocus technique is investigated as a means of expanding the range-squint angle boundaries of synthetic aperture radar operation.

Development

The differences in Real and Synthetic Aperture Radar are first discussed giving the reader a refresher in radar theory and leading to discussion of aperture length and integration time requirements as well as SAR focusing and aperture weighting. SAR phase errors and image quality will then be covered with particular attention being given to phase errors caused by SAR aircraft

motion measurement errors and their visual effects. Unaided INS error characteristics will then be explored showing the feasibility of a one nautical mile per hour INS for performing the motion compensation requirements. Then aided INS performance capabilities are demonstrated for typical strapdown Inertial Navigation Systems such as the SPN-GEANS, N-73, or Ring Laser Gyros. The previous sections have merely been designed to show the conceptual compatibility between strapdown INS performance and SAR motion compensation requirements. Next, SAR motion compensation requirements are covered to illustrate the INS performance necessary to achieve the quadratic phase error required for SAR focusing for specific operating conditions. Once the compatibility between INS performance and SAR motion compensation requirements have been shown, it is still necessary to use some sort of focusing technique to obtain high resolution images under more severe aircraft maneuvering. This study is concluded with an explanation of the Autofocus technique for motion compensation giving SAR performance envelopes with and without the Autofocus process being used.

II. Real and Synthetic Radar

Real array imaging radars obtain y-direction resolution by virtue of the real antenna beam coverage on the ground which is determined by the physical size of the antenna. The y-direction being the along track or direction in which the aircraft is moving. Finer resolution will require longer antennas, which because of their size can only be mounted lengthwise along the aircraft. This results in an antenna beam looking to the side of the aircraft. As will be seen later, incremental Doppler shift of adjacent resolution cells in the y-direction can only be separated if the antenna is looking to one side rather than straight ahead. This is typically the method used in reconnaissance aircraft and not useful in an aircraft engaged in weapon delivery or navigation updating with which this study is concerned. To make synthetic radars useful in tactical applications, the radar will have to look slightly to the side rather than straight ahead. This angle between the direction the aircraft is moving and the direction in which the radar is looking will be called the squint angle.

Figure 2.1 shows a simplified diagram of the geometry of a real array imaging radar. The aircraft flies along the y-direction at velocity V . Its long antenna produces a fan beam which illuminates the ground below. For simplicities sake, the squint angle is taken to be ninety degrees. It is important to note that the beams width is narrower in the y-direction than its length in the x-direction. The y-direction resolution is determined by the beamwidth while the x-direction resolution is determined by the pulse length and is independent of the beamwidth. In an aircraft using real imaging radar, the antenna alternately transmits and receives energy and displays the ground returns received on a cathode ray tube or records the images on film. The resolution needed to determine objects will be covered first.

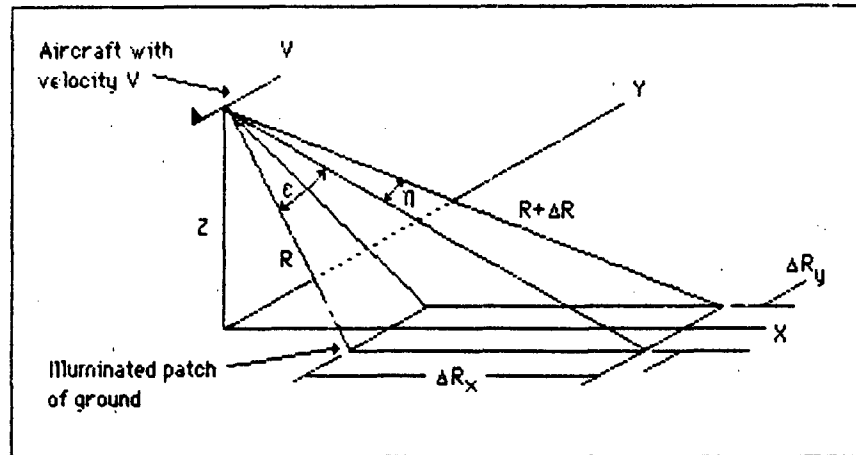


Fig. 2.1 Geometry of a Real Array Imaging Radar (17:33)

Resolution Cell Size

It should be helpful to discuss required resolution for determining objects before covering achievable radar mapping resolution. Table 2.1 gives the required resolution cell sizes for various objects. Large objects, such as coastlines, cities, and mountains, can be recognized with 150m resolution elements. Vehicles, houses, and buildings however need resolution elements along the order of 3 meters. This gives a reference for determining the resolution required to go after certain targets using a tactical aircraft.

TABLE 2.1 RESOLUTION CELL SIZE FOR VARIOUS OBJECTS (13:3)

ITEM	SQUARE CELL SIZE (meters)
Coastlines, Cities, Mountains	150
Major Highways, Large Airfields	30
City Streets, Large Buildings	15
Vehicles, Houses, Buildings	3

X-Direction Resolution

Pulse radars measure range by transmitting a pulse and timing the returned pulse from

the target. Figure 2.2 shows this relationship with pulse duration τ and an interpulse period of T . The aircraft geometry in the vertical plane is also shown by Figure 2.3. The squint angle is again assumed equal to ninety degrees.

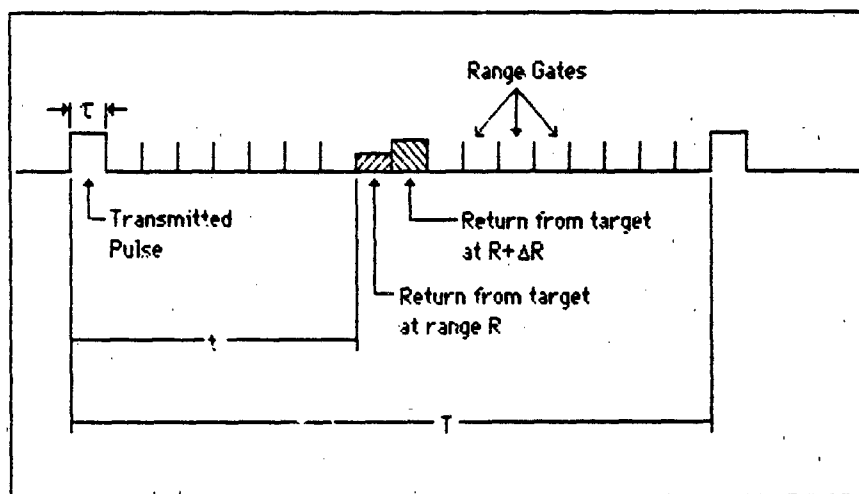


Fig. 2.2 Radar Range Gates (13:5)

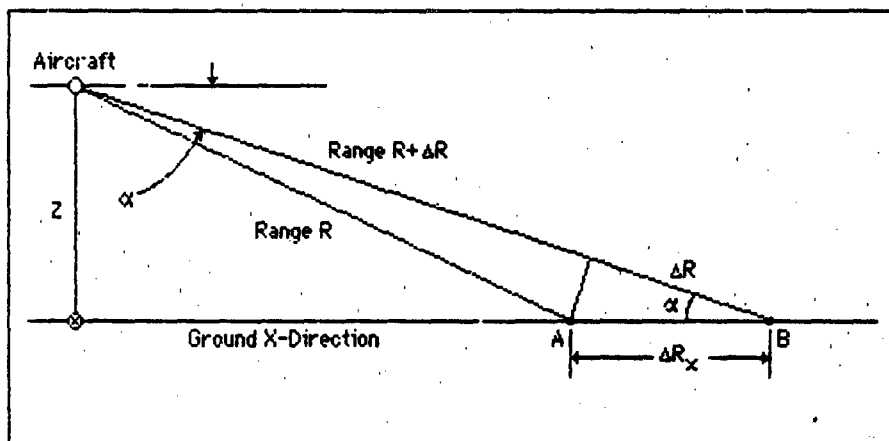


Fig. 2.3 Resolution in the X-Direction (13:5)

If the range gates are of duration τ , two adjacent points on the ground, A and B, which are ΔR_x apart, can be resolved by their returns occurring in two adjacent range gates as shown. Electromagnetic energy travels at the speed of light, c , so the time for the energy to travel to the target and return is given by

$$t = \frac{2R}{c}; \quad t + \tau = \frac{2(R + \Delta R)}{c} \quad (\text{sec}) \quad (2.1)$$

Subtracting equations (2.1) gives

$$\tau = \frac{2\Delta R}{c} \quad (\text{sec}) \quad (2.2)$$

and from observation of Figure 2.3

$$\Delta R_x = \frac{\Delta R}{\cos \alpha} = \frac{c\tau}{2\cos \alpha} \quad (\text{m}) \quad (2.3)$$

where ΔR_x is the resolution in the x-direction or perpendicular to the ground track. It can be seen from equation (2.3) that resolution in the x-direction is directly proportional to the pulsewidth τ . Therefore, shorter pulsewidths produce better resolution. In radars which are matched, i.e. the product of pulse duration τ and the receiver bandwidth W is unity, one gets

$$\Delta R_x = \frac{c\tau}{2\cos \alpha} = \frac{c\left(\frac{1}{W}\right)}{2\cos \alpha} = \frac{c}{2W\cos \alpha} \quad (\text{m}) \quad (2.4)$$

In the pulse radar shown in Figure 2.2, the maximum measurable range R_{max} is a function of interpulse period T , and is given by

$$R_{\max} = \frac{cT}{2} \quad (\text{km}) \quad (2.5)$$

If R is beyond this range, the elapsed time between transmitted pulse and target return pulse will include multiples of interpulse period T , making the measured range ambiguous.

Y-Direction Resolution

In real array imaging radars resolution in the y -direction is proportional to the antenna beamwidth. A rectangular antenna with uniform current distribution will produce a $(\sin x)/x$ antenna pattern (4:385-389, 12:2-20). The approximate expressions for half-power beamwidth of this antenna are

$$\eta = \frac{51\lambda}{l_1}, \quad \epsilon = \frac{51\lambda}{l_2} \quad (\text{degrees}) \quad (2.6)$$

where η and ϵ are half-power beamwidths in degrees, λ is the wavelength and l_1 and l_2 are the sides of the antenna. A circular antenna with uniform current distribution will produce a radiation field intensity involving first order Bessel functions (12:2-24). The half-power beamwidth in this case will be

$$\gamma = \frac{58.5\lambda}{D} \quad (\text{degrees}) \approx \frac{\lambda}{D} \quad (\text{radians}) \quad (2.7)$$

where γ is the half-power beamwidth and D is the diameter of the antenna. In further discussion the value of γ will be approximated by $\gamma = \lambda/D$ where γ is given in radians. It is now easy to determine the resolution in the y -direction. From Figure 2.1 the resolution in the y -direction is

$$\Delta R_y = R\eta \quad (m) \quad (2.8)$$

where ΔR_y is the resolution in the y-direction, R is the range to the resolution cell and η is antenna azimuth beamwidth. If the value of η is approximated by λ/l_1 , the resolution in the y-direction is given by

$$\Delta R_y = \frac{R\lambda}{l_1} \quad (m) \quad (2.9)$$

As seen by equation (2.9), the resolution in the y-direction is dependent on range R. Therefore as the range gets smaller, resolution improves. This property in real array imaging radars make ground points closer to the aircraft resolvable while points further away merge together. In both real and synthetic array imaging radars, resolution in the x-direction depends on the time of arrival of the target return signal. Because of this phenomenon, equidistance points from the radar will all converge to the same range gate and these points will all occur at the same x-resolution cell. To someone at the position of the aircraft, these points will show up at three distinct locations.

The need for ground maps without using large antennas led to synthetic array radars. These radars use pulse duration, as in the case of real array imaging radars, for x-direction resolution. However, y-direction resolution is determined by using Doppler shifts or spectral analysis as opposed to beamwidth. Therefore, the long antenna producing a narrow beam is replaced in the synthetic radar by a great deal of spectral signal processing. By using synthetic signal processing techniques one can obtain high resolution ground maps using standard antennas in aircraft. Since the basis of resolution in the y-direction is frequency shift, which is the rate of change of phase, a discussion of these topics will be given.

If a transmitted waveform given by

$$V_t = \sin 2\pi f_0 t \quad (\text{m/sec}) \quad (2.10)$$

is emitted from an antenna and this signal is reflected from a moving target with radar-target range R given by the equation

$$R = R_0 + \dot{R}t \quad (\text{km}) \quad (2.11)$$

where R_0 is the initial range, \dot{R} is target's closing rate in the direction of R , and t is the time.

The returned signal at time t will be the signal which was transmitted Δt seconds ago with Δt given by t in equation (2.1). If one substitutes $t=t-\Delta t$ in (2.10) the received signal is

$$V_r = \sin \left[2\pi f_0 \left(t - \frac{2R_0 + 2\dot{R}t}{c} \right) \right] \quad (\text{m/sec}) \quad (2.12)$$

Once terms involving t are grouped together

$$V_r = \sin \left[\left(2\pi f_0 - \frac{2\dot{R}(2\pi f_0)}{c} \right) t - \frac{2(2\pi f_0)R_0}{c} \right] \quad (2.13)$$

Notice that the coefficient of time t in the argument represents frequency while the part not involving time represents a phase ϕ . The frequency and phase of the returned signal will be

$$2\pi f_r = 2\pi f_0 - \frac{2\dot{R}(2\pi f_0)}{c}, \quad \phi_r = -\frac{2(2\pi f_0)R_0}{c} \quad (2.14)$$

To obtain the difference of transmit and receive frequencies, $f_r - f_0$, equation (2.14) is rearranged to arrive at

$$f_d = f_r - f_0 = \frac{-2\dot{R}(f_0)}{c} = \frac{-2\dot{R}}{c/f_0} = \frac{-2\dot{R}}{\lambda} \quad (\text{Hz}) \quad (2.15)$$

where f_d is recognized as the doppler shift and c/f_0 is the wave length λ . It can be seen that the return from a moving target will be shifted in frequency directly proportional to radar-target closing rate and inversely proportional to wavelength. Also, the phase angle of the returned signal ϕ_r as given by (2.14) can be written as

$$\phi_r = -(2\pi) \frac{2R_0}{c/f_0} = \frac{-4\pi R_0}{\lambda} \quad (\text{radians}) \quad (2.16)$$

Equation 2.16 represents the number of equivalent wavelengths to the round trip distance $2R_0$. The factor of 2π converts the number of wavelengths to angles in radians. Therefore, the phase change is equivalent to a distance. Similarly, the Doppler shift of equation (2.15) for an incoming target can be interpreted as the number of wavelengths/second that the transmitted signal is pushed in due to the closing rate \dot{R} . The number of wavelengths/second is recognized to be frequency. To summarize, it should be noted that phase is associated with range while the derivative of phase with respect to time (frequency) is associated with range rate.

Again, resolution in the y -direction is looked at. Using Figure 2.4, an aircraft flying at velocity V parallel to the y -axis attempts to differentiate between points A and B. To do this, the

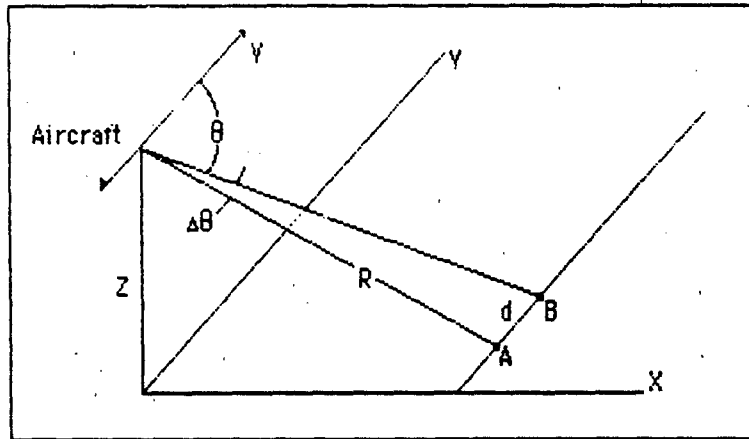


Fig. 2.4 Resolution of Two Points a Distance d Apart

frequency difference between the two ground points A and B, which are a distance d apart, is obtained. Using the previous equations and Figure 2.4 the Doppler shifts for the points are extracted.

$$f_B = \frac{2V \cos \theta}{\lambda} \quad f_A = \frac{2V \cos(\theta + \Delta \theta)}{\lambda} \quad (\text{Hz}) \quad (2.17)$$

If $\cos(\theta + \Delta \theta)$ is expanded in terms of sines and cosines and using the small angle relationships of $\cos \Delta \theta \cong 1$ and $\sin \Delta \theta \cong \Delta \theta$, the differences in frequency are

$$\Delta f_i = f_B - f_A = \frac{2V}{\lambda} \Delta \theta \sin \theta \quad (\text{Hz}) \quad (2.18)$$

From Figure 2.4 $\Delta \theta$ can be approximated by

$$\Delta \theta \cong \frac{d}{R} \quad (2.19)$$

where R is the range. If equation (2.19) is used in (2.18)

$$\Delta f_i = \frac{2Vd}{\lambda R} \sin \theta \quad (\text{Hz}) \quad (2.20)$$

Therefore resolution in the y-direction becomes.

$$\Delta R_y = d = \frac{\lambda R \Delta f_i}{2V \sin \theta} \quad (m) \quad (2.21)$$

The resolution attained above is independent of antenna beamwidth (as was not the case in real array imaging radars) and depends primarily on attainable frequency resolution Δf_i of the signal processing equipment. Again for a matched transmit/receive system the duration of target illumination T should be $1/\Delta f_i$. What this means is that during the data acquisition time T the aircraft flies a length of $L=VT$ where V is its velocity. Thus, it can be seen the equivalent antenna array length becomes

$$L = VT = \frac{V}{\Delta f_i} = \frac{\lambda R}{2d \sin \theta} \quad (m) \quad (2.22)$$

Using the value of L from (2.22) another value of y-direction resolution is obtained.

$$\Delta R_y = d = \frac{\lambda R}{2L \sin \theta} \quad (m) \quad (2.23)$$

This value of y-direction resolution is the best attainable and is used as a measure of merit in further calculations. In actual practice, the y-direction resolution is obtained by a set of tuned filters as shown in Figure 2.5. This figure shows a set of filters with a $(\sin x)/x$ drop-off

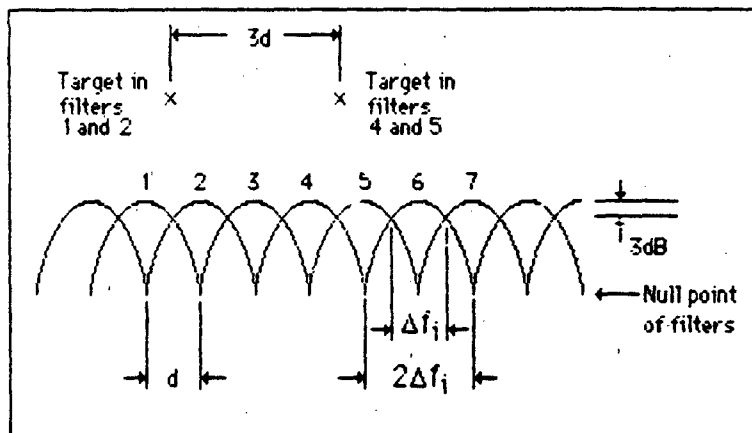


Fig. 2.5 Actual and Theoretical Y-Direction Resolution (13:20)

characteristics. The 3-dB bandwidths of the filters in Fig. 2.5 are approximately one-half of the null-to-null bandwidth. Referring to Fig. 2.5, a typical target will, fall into two adjacent filters, e.g., filters 1 and 2. Averaging will put the target in the center of these filters as shown. To obtain proper resolution separation filter number 3 should be skipped and the next resolvable target will probably appear in filters 4 and 5. Averaging will put the target between these filters as shown. Thus, it can be seen that the practical attainable resolution is $3d$.

Going back to equation (2.22), representative SAR integration times and aperture lengths can be determined as shown in Table 2.2.

Table 2.2 Representative Integration Times and Aperture Lengths

Tactical Conditions	Azimuth Res (m)	Integration Times (sec)	Synthetic Aperture (m)
$\theta = 90^\circ$	1	1.74	485
$V = 912 \text{ ft/sec}$	3	.58	162
$= 540 \text{ knots}$	10	.17	48
$\theta = 20^\circ$	1	6.12	1417
$V = 760 \text{ ft/sec}$	3	2.04	472
$= 450 \text{ knots}$	10	.61	142
$\lambda = 106 \text{ ft} \quad R = 30 \text{ km}$			

III. SAR Focusing and Aperture Weighting

The concept of focusing is fundamental to motion compensation and high resolution SAR. There are several analytical approaches which are possible when considering the topic of focusing. Among these are vector addition, cross correlation, and matched filtering. All these techniques give approximately the same results. The approach which will be followed here is that of real beam antenna theory in which the field intensity pattern of the antenna is related to the current distribution across the aperture by the Fourier transform. If the parabolic reflector real beam antenna of Figure 3.1 is considered, it can be seen that any ray from the focus is reflected in a direction parallel to the axis of the parabola. The distance traveled by any

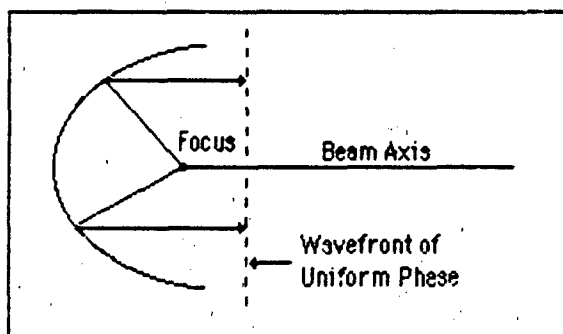


Fig. 3.1 Parabolic Reflector

ray from the focus to the parabola and by reflection to a plane perpendicular to the parabola axis is independent of its path. This characteristic results in a point source of energy located at the focus being converted into a plane wave of uniform phase. Note the similarity of Figure 3.2 to that of Figure 3.1. A circular flight path with its origin at the map point would also result in a SAR aperture distribution having uniform phase. If it were possible to maintain this flight path the SAR aperture would be focused and no motion compensation would be necessary. This type

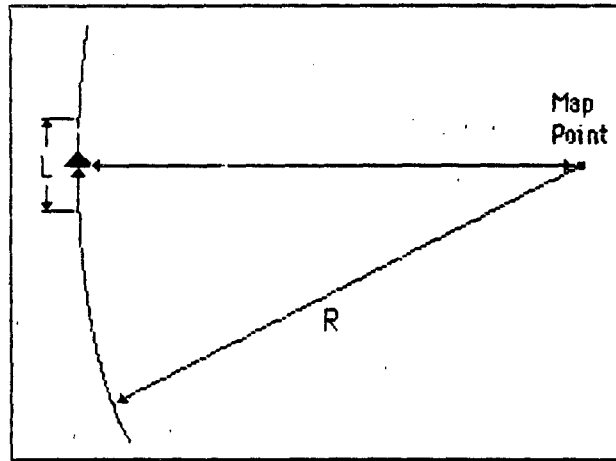


Fig. 3.2 Uniform Phase Aircraft Flight Profile

of flight path is impossible to maintain and is in fact tactically unacceptable, therefore motion compensation must be used to compensate the phase of each transmitted radar pulse such that an effective synthetic aperture is realized having uniform phase across its length. The electric field intensity pattern, $E(\phi)$, can be obtained as the Fourier transform of the current distribution across the aperture. This pattern can be determined for an aperture distribution of uniform phase and constant amplitude as

$$E(\phi) = \int_{-L/2}^{L/2} A(Y) e^{j2\pi Y \sin \phi / \lambda} dY = A_0 \int_{-L/2}^{L/2} e^{j2\pi Y \sin \phi / \lambda} dY \quad (3.1)$$

$$E(\phi) = \frac{\sin[\pi(L/\lambda)\sin \phi]}{\pi(L/\lambda)\sin \phi} = \frac{\sin x}{x} \quad (3.2)$$

where L is the length of the aperture in the Y direction and ϕ is the azimuth angle measured from a normal to the Y direction. If the square of $E(\phi)$ is plotted, the power radiation pattern

would be obtained as shown in Figure 3.3. This should be familiar as the $(\sin x)/x$ pattern. This pattern is applicable for both the real beam parabolic antenna of Figure 3.1 and the synthetic aperture antenna of Figure 3.2. Resolution of either antenna is inversely proportional to the aperture's length. It should be noted that the radiation pattern corresponding to uniform

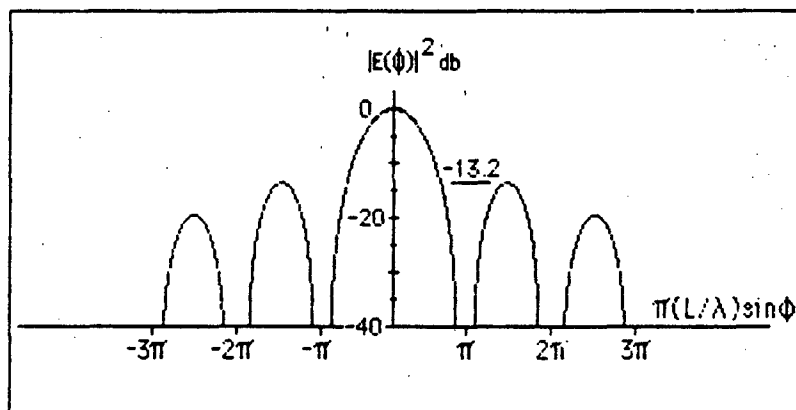


Fig. 3.3 Radiation Pattern for Uniformly Illuminated Arrays

amplitude distributions has a peak side-to-main lobe ratio of -13.2 db. These high side lobes will adversely affect the quality of SAR imagery by filling in low radar return terrain, such as roads, rivers, lakes, and runways, with energy coming in through the side lobes from potentially high radar backscattering terrain such as trees, rocks, and buildings. This characteristic has the effect of reducing contrast or washing out the SAR map. This problem can be improved by reducing the side lobe level through tapering or weighting the aperture amplitude distribution to decrease as a function of distance from the center. However, the reduction of the sidelobes increases the width of the main lobe.

IV. SAR Phase Errors and Image Quality

The ability to achieve a perfectly uniform phase distribution across the aperture is unrealistic in practice due to the many ways in which phase errors can occur in SAR systems; atmospheric propagation, transmitter nonlinearities, instabilities, motion compensation, etc. The phase errors which occur affect system performance by degrading the antenna radiation pattern, and more generally, the system impulse response which additionally includes the range dimension. As phase errors increase, the system impulse response is degraded in many ways; the sidelobe levels are increased, the mainlobe width is increased resulting in a loss of resolution, and the mainlobe peak is reduced. This study is primarily interested in phase errors caused by aircraft INS motion measurement errors. The effects produced by these phase errors are most easily analyzed by separating them into two types; low and high frequency. Figure 4.1 depicts these errors.

Frequency	Phase Error		
Low	Fixed	Linear	Quadratic
Medium	Cubic	Quartan	Quintan
High	Sinusoidal	Random	

Fig. 4.1 Types of SAR Phase Errors

Low Frequency Errors

The low frequency errors exhibit less than one cycle variation over the processing aperture and can be represented as a Taylor series.

$$\psi(t) = \frac{4\pi R(t)}{\lambda} \quad (4.1)$$

$$\psi(t) = \frac{4\pi}{\lambda} \left[R(0) + \left(\frac{\partial R}{\partial t} \right) t + \left(\frac{\partial^2 R}{\partial t^2} \right) \frac{t^2}{2!} + \dots \right] \quad (4.2)$$

where: $R(0)$ = the SAR aircraft-to-map point range at the beginning of the coherent integration time interval.

t = the time referenced to the start of coherent integration.

The error in the first term of Eq. 4.2 which is time independent must be small enough to permit illumination of the proper area to be mapped, cue the target, and meet the weapon delivery requirements. The error in the second term of Eq. 4.2 which is linear in time and distance results in an azimuth shift of the system impulse response but does not otherwise degrade it. In the radar "open-loop" the SAR map is tracked in both azimuth angle and Doppler and therefore the magnitude of the second term must be small enough to insure that the antenna illuminates the same ground patch that the signal processor is filtering. The error in the third term of Eq. 4.2 is by far the most important and generally produces all the degrading effects described earlier. These effects are shown in Figure 4.2 where the phase error is from the center to the edge of the aperture. The higher order low frequency phase errors affect the system impulse response in the same manner as the quadratic phase error (QPE) but their magnitudes are greatly reduced and do not limit system performance.

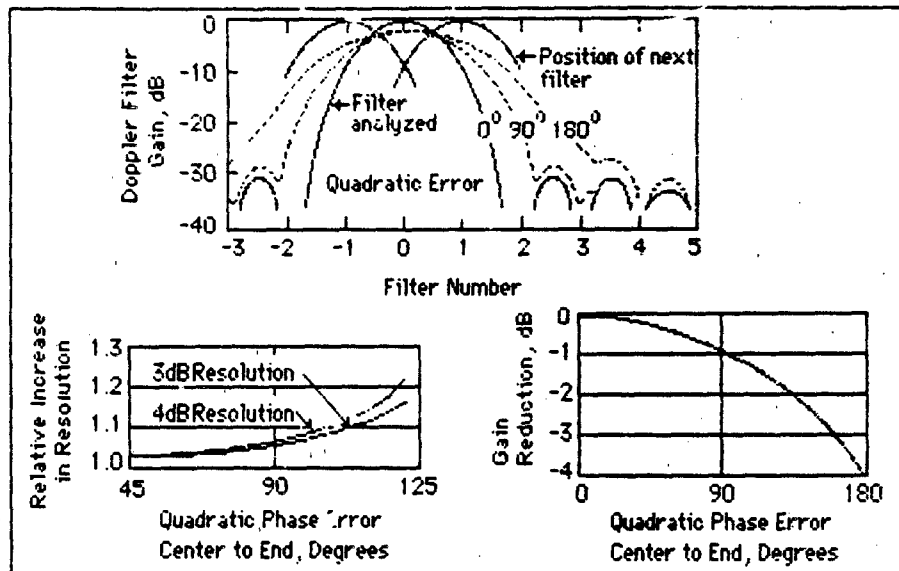


Fig. 4.2 Effect of Quadratic Phase Error on Resolution and Gain (16:9)

High Frequency Errors

The effects of high frequency sinusoidal phase errors on a SAR impulse function response has been known for some time under the theory of paired echos. The following expression is a good approximation to the azimuth channel response $v(x)$ of a SAR system for a peak sinusoidal phase error of one radian or less.

$$v(x) = J_0(\psi)v_0(x) + jJ_1(\psi)\left[v_0\left(x - \frac{\omega}{k}\right) + v_0\left(x + \frac{\omega}{k}\right)\right] \quad (4.3)$$

where ψ is the phase error amplitude, ω is the phase error radian frequency, J_m is the Bessel function of the first kind and of order m , $v_0(x)$ is the desired response, x is the azimuth distance, and $k=4\pi/\lambda R$. The desired response is reduced in amplitude by the amount $J_0(\psi)$ and

is surrounded with a pair of echoes with displacements of ω/k as shown in Figure 4.3.

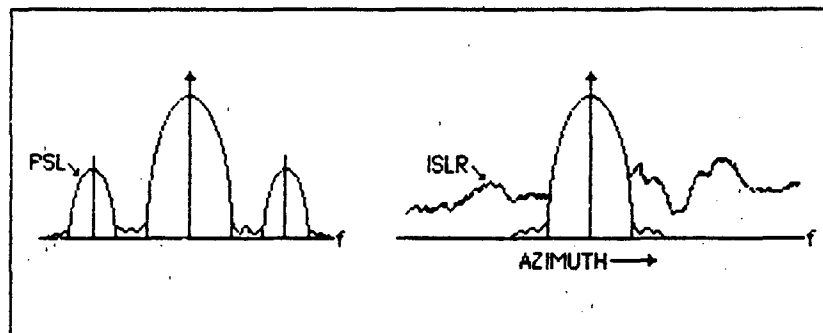


Fig. 4.3 Side Lobe Energy Due to High Frequency Phase Errors

Since phase-corrupted and phase-error-free outputs have equal energies, energy is removed from the main lobe and redistributed in the sidelobes. Increase in the side lobe levels is undesirable since it leads to spurious target responses and poor image contrast. The peak side lobe to main lobe ratio (PSLR) is given by:

$$\text{PSLR} = \left| \frac{J_1(\psi)}{J_0(\psi)} \right|^2 = \frac{1}{4} \left[\frac{\psi^2(1-\psi^2/4)}{1-\frac{\psi^2}{2} + \frac{3\psi^4}{32}} \right] \quad (4.4)$$

The primary effect from high frequency random phase errors is also shown in Figure 4.3 and is to take main lobe energy and distribute it over several side lobes rather than concentrating the energy as sinusoidal phase errors do. An analysis of the integrated side lobe energy shows that its ratio relative to the main lobe (ISLR) is approximated by the variance of high frequency phase errors for errors a third of a radian or less:

$$ISLR = \frac{ISLE}{MLE} = \sigma_{\psi}^2 \quad (4.5)$$

Summary

To tie this section on SAR phase errors together, their qualitative effect on image quality is considered and can be shown via Figure 4.4. Quadratic phase error (QPE) causes broadening of the image processing system's impulse response width. For 90 degrees of QPE measured from the center of a coherent array to its end (sometimes called the Rayleigh limit), the main lobe

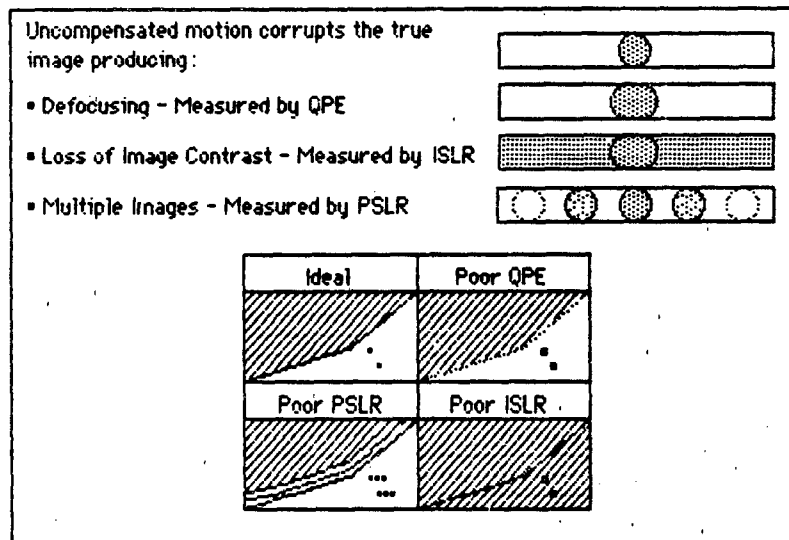


Fig. 4.4 Visual Effects of Poor QPE, PSLR, and ISLR (16:12)

width is increased by about 8 percent for a uniformly weighted array. This broadening causes an effective decrease in image resolution and tends to smear targets. However, the effect of QPE is not limited to the main lobe. One of its first effects is to fill in side lobe nulls and increase ISLR causing some of the same visual effects that ISLR does. When error levels are sufficiently high, PSLR problems are probably the easiest to observe and identify. Multiple images appear

in the map as if various shifted versions of the true scene were overlaid on top of one another. Increased PSLR is also accompanied by degraded ISLR but ISLR problems are more often the result of phenomena more distributed in frequency which causes an overall increase in side lobe levels without distinctive side lobe peaks. This side lobe corruption may be so severe that it obliterates edges and contrast boundaries in the scene. The image appears washed out.

V. INS Characteristics and Capabilities

Navigation by the process of determining position from self contained inertial measurements made on board the aircraft is termed inertial navigation. A typical Inertial Navigation System consists of gyros, accelerometers, a computer, and associated equipment. The gyros are used to establish an inertial reference frame. The components of inertial acceleration as measured in this reference frame are determined from the outputs of accelerometers after accounting for the effect of gravity on the measurements. Then a single integration gives the velocity and another integration gives the position of the aircraft. It can be demonstrated that the propagation of errors in an INS is very accurately described by a set of linear differential equations under a very broad set of assumptions (26). The minimum number of equations necessary to simulate the INS errors is nine; three each for velocity, position, and attitude errors. These are the familiar Pinson error states. If additional INS hardware and various computational errors are to be simulated, the number of simultaneous error equations required increases on a one-for-one basis.

Unaided INS

The typical military aircraft of today contain an INS having an accuracy of approximately one nautical mile (nm) per hour when operated in the pure inertial unaided mode. A characteristic of this class of INS is that its navigational accuracy is determined and limited by the gyros whose technology has resulted in an error performance of approximately 0.01 degrees per hour drift rate. While there are at least one hundred hardware mechanizations and software computational error sources that contribute to the navigation errors, these are generally controlled such that the gyro drift rate errors limit INS accuracy. Figure 5.1 illustrates

typical INS error performance for a local level platform mechanization having a north gyro drift rate error of 0.01 degrees per hour (26:61). These characteristics were obtained by simulating a set of ten simultaneous differential equations. The error performance indicated is

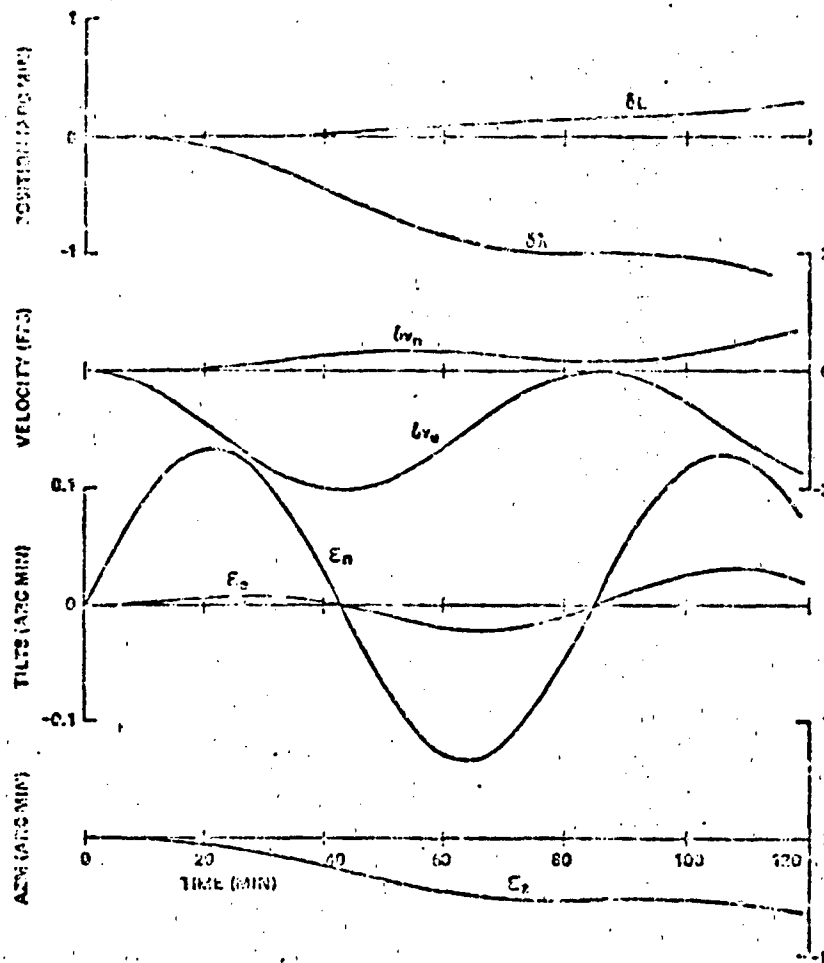


Fig. 5.1 Typical INS Navigation Errors (26:61)

of the correct order of magnitude for a one nm INS. Other error sources, including alignment, would tend to modify these characteristics but would also result in platform tilt errors.

exhibiting the 84 minute period Schuler oscillations. An exception to the above error sources would be the situation of violent aircraft maneuvers coupled with acceleration sensitive gyro drift rate errors.

Determining the feasibility of a one nm per hour INS for performing the motion compensation function depends to a large extent on the time dependent linear, quadratic, and higher order position error components. The "order of magnitude" amplitude of these components can be determined by expanding the longitude error of Figure 5.1 into a Taylor series. To accomplish this expansion, the east velocity error, δv_e , is approximated by:

$$V_e = \cos(\omega t) - 1 \quad (\text{ft/sec}) \quad (5.1)$$

where t is time in seconds, ω is $2\pi/T_s$ and T_s is the Schuler period of 5040 seconds. The east position (longitude) error is found as the integral of the velocity error:

$$P_e = \int_0^t [(\cos \omega t) - 1] dt = \frac{\sin \omega t}{\omega} - t \quad (\text{ft}) \quad (5.2)$$

The precision of the position information ΔP_e , rather than absolute accuracy, over a SAR coherent integration interval ΔT , is the quantity of interest here. So,

$$\Delta P_e(\Delta T) = P_e(t) - P_e(t + \Delta T) \quad (\text{ft}) \quad (5.3)$$

Substituting equation 5.2 into 5.3 and expanding the $\sin(t + \Delta T)$ term results in

$$\Delta P_e(\Delta T) = \Delta T + \frac{1}{\omega} [\sin \omega t - \sin \omega t \cos \omega \Delta T - \cos \omega t \sin \omega \Delta T] \quad (5.4)$$

Now this position error can be expanded into its low and higher order time components by the use of Taylor series expansions and specific values of time:

$$\cos \omega \Delta T = 1 - \frac{(\omega \Delta T)^2}{2!} + \frac{(\omega \Delta T)^4}{4!} - \frac{(\omega \Delta T)^6}{6!} + \dots \quad (5.5)$$

$$\omega t = \frac{\pi}{2}, \frac{5\pi}{2}, \frac{9\pi}{2}, \dots \quad (5.6)$$

to arrive at

$$\Delta P_e = \Delta T + \frac{1}{\omega} \left[\frac{(\omega \Delta T)^2}{2!} + \frac{(\omega \Delta T)^4}{4!} - \frac{(\omega \Delta T)^6}{6!} + \dots \right] \quad (ft) \quad (5.7)$$

In a similar manner:

$$\sin \omega \Delta T = \omega \Delta T - \frac{(\omega \Delta T)^3}{3!} + \frac{(\omega \Delta T)^5}{5!} - \frac{(\omega \Delta T)^7}{7!} + \dots \quad (5.8)$$

$$\omega t = 0, 2\pi, 4\pi, 6\pi, \dots \quad (5.9)$$

$$\Delta P_e = \frac{1}{\omega} \left[\frac{(\omega \Delta T)^3}{3!} - \frac{(\omega \Delta T)^5}{5!} + \frac{(\omega \Delta T)^7}{7!} - \dots \right] \quad (ft) \quad (5.10)$$

Representative values of these time dependent errors are given in Table 5.1 for a one nm per hour INS with a coherent integration time of 3.5 seconds. These position error components are

TABLE 5.1 REPRESENTATIVE INS POSITION ERRORS

Time Dependency	Aircraft Motion	Error Magnitude (ft)
Linear	Velocity	3.5
Quadratic	Acceleration	.00764
Cubic	Jerk	.00001

seen to drop off rapidly with increasing order and it is this very characteristic which makes an INS a feasible motion compensation sensor. As seen previously, SAR image quality will largely be determined by the quadratic and higher order components. Table 5.1 shows that these components are relatively small when compared to a wavelength of .106 feet at X-band.

Aided INS

While it has been shown that a nominal one nm per hour INS has an inherent capability to provide the desired motion sensing for many SAR applications, it is possible that there are difficult mapping conditions (long range, high resolution, aircraft maneuvers, etc.) where higher INS performance would be desirable in order to focus the SAR. An aided inertial Kalman filter INS mechanization utilizing velocity and position updates affords a means of greatly enhancing INS performance with regard to reducing quadratic phase errors. Table 5.2 provides an assessment of state-of-the-art aided INS performance where various position and/or velocity measuring sensors have been integrated with a high accuracy 0.1 nm per hour INS. The system's ability to accurately measure aircraft acceleration, velocity, and position is shown and corresponds to a rather long 30 minute ground alignment and a short 20 minute flight time. The radar position accuracy given reflects INS state immediately after the measurement. A top level error budget showing the various contributors to the acceleration measurement errors of Table 5.2 is given in Table 5.3. Data is given for straight and level flight and a 6g maneuver. The

TABLE 5.2 PROJECTED AIDED INS PERFORMANCE (16:17)

AIDED INS MECHANIZATION	MEASUREMENT ERROR			
	Acceleration (μg)		Velocity (m/sec)	Position (meters)
	Level Flight	6g Maneuver		
Master-Slave or Improved Strapdown				
Unaided System	112	715	.3	75
Radar Altimeter-DLMS Aiding	112	715	.3	75
GPS Aiding (Type 1)	50	874	.06	6
Velocity Update & Star Fix	112	715	.1	75
Unconv. Gnd. Align	112	500	.3	75
Radar Position Update	112	715	.3	12-23
Current State-of-the-Art Strapdown (Laser Gyros)				
Unaided System	137	3158	1	525
Radar-DLMS Aiding	137	3158	1	75
GPS Aiding	50	874	.06	6
Radar Aiding & Star Fix	137	715	.6	450
Unconv. Gnd. Align	137	3158	1	12-23

accelerometer null shift bias, scale factor, nonorthogonality, and mechanical misalignment errors determine the residual verticality errors after ground alignment. The major error in the gyrocompass ground alignment is an azimuth misalignment caused by the east component of the 0.001 degree per hour gyro drift rate. It is important to point out that gravity anomalies affect INS accuracy because accelerometers do not measure acceleration directly. They measure specific force, which is the vector difference between acceleration and gravity. Therefore, it is necessary to compute the gravity vector, and to add it to the vector output of an accelerometer triad in order to obtain a measure of acceleration. The computation of the gravity vector entails the use of an imperfect mathematical model of the earth's gravity field. The errors in this model are the gravity anomalies. The current state-of-the-art in gravity models is such that the anomalies have 6.3 arc sec deflection (errors in the along-track and cross-track direction),

TABLE 5.3 ACCELERATION MEASUREMENT ERROR BUDGET (16-18)

ERROR	1 σ Value	CONTRIBUTION TO MEASUREMENT ERROR (μ g)	
		6g	Maneuvering
1. Gravity Anomalies			
a. RSS Deflection	9 arc sec	43	43
b. Magnitude	68 μ g	68	68
2. Accelerometer Errors	50 μ g	50	50
3. RSS Accelerometer Platform Drift	0.001 deg/hr	60	10
4. Accelerometer Platform Ground Alignment			
a. RSS Verticality (Accelerometer Error)	141 μ g	425	71
b. Azimuth Misalignment (East Gyro Drift Rate During Gyrocompassing)	0.001 deg/hr	564	0
RSS		<u>715</u>	<u>112</u>

and 67.5 micro-g magnitude error in the vertical direction. The 6.3 arc sec gravity deflections are equivalent to a 43 micro-g acceleration error in the horizontal plane. Nothing can be done at present about this kind of error by making better accelerometers and gyros.

VI. SAR Motion Compensation Requirements

It has been shown in the previous sections that the conceptual compatibility exists between INS performance and SAR motion compensation requirements. This section will explore the INS performance necessary to achieve the QPE required for SAR focusing in various specific operating conditions. A major source of quadratic phase error is caused by an uncompensated acceleration along the line-of-sight (LOS) to the map-point. This distance error is the product of one half the acceleration error and time squared and is a quadratic function. This LOS acceleration is made up of two components; (1) centripetal acceleration due to ideal straight line motion of the radar as it flies past the map reference point, and (2) that due to maneuvers or disturbances from the ideal flight path. From the first of these two components, an uncompensated error occurs when the INS has a velocity error component normal to the LOS to the map reference point. An uncompensated error from the second component results when the INS has LOS acceleration measurement error.

Although these QPE are fundamental to INS and SAR integration, there are other sources of QPE which can arise. It can be shown that bistatic SAR incurs a rather severe QPE due to illuminator and receiver position errors and also from stable oscillator frequency differences. Imperfect radar system mechanizations, of which there are many, may result in a time delay between the sensing and application of motion data during aircraft maneuvers causing a very substantial QPE. These and other potential sources of QPE must be considered in a system level error budget for any given SAR design but will not be covered in this study.

LOS Acceleration Measurement Error

In order to relate the required INS acceleration measurement accuracy to SAR azimuth resolution, aircraft motion, and scenario parameters, an equation is derived for the LOS

acceleration measurement accuracy. The INS requirement which results is then compared to current INS performance capabilities to determine the nominal SAR operating boundaries imposed by this particular motion compensation error. In order to get the equation for the LOS acceleration measurement accuracy the quadratic term of the Taylor series expansion in Equation 4.2 is substituted into the expression for phase error as given by Equation 4.3.

$$\Delta\psi_q(t) = \frac{2\pi}{\lambda} \dots JS^2 \quad (\text{radians}) \quad (6.1)$$

$$\Delta\psi_q(T/2) = \frac{\pi}{2\lambda} \Delta a_{\text{LOS}} T^2 \quad (\text{radians}) \quad (6.2)$$

where:

$$\Delta a_{\text{LOS}} \triangleq \frac{\partial^2 \Delta R(t)}{\partial t^2} \quad \text{and} \quad t = \frac{T}{2} \quad (6.3)$$

If Equation 2.22 is rearranged to obtain the coherent integration time and a permissible quadratic phase error of 90 degrees is used

$$\Delta\psi_q(T/2) = \frac{\pi \lambda R^2}{8d^2 V^2 \sin^2 \theta} \Delta a_{\text{LOS}} = \frac{\pi}{2} \quad (\text{radians}) \quad (6.4)$$

$$\Delta a_{\text{LOS}} = \frac{4d^2 V^2 \sin^2 \theta}{\lambda R^2} \quad (\text{ft/sec}) \quad (6.5)$$

It must be remembered that this expression for the LOS acceleration measurement accuracy is optimistic in that it requires the entire error budget and makes no allowance for a centripetal acceleration or other QPE components. Required acceleration measurement accuracy vs. squint

angle is tabulated in Table 6.1 to show the increasing accuracy needed as the squint angle decreases. Also, in Table 6.2, the acceleration measurement accuracy vs. tactical aircraft speed is tabulated showing the increasing accuracy needed as aircraft speed decreases. A comparison of the motion compensation requirements of Tables 6.1 and 6.2 and the acceleration measurement accuracy performance of Table 5.2 indicates that a state-of-the-art, 0.1 nm per hour, aided INS

TABLE 6.1 LOS ACCELERATION ACCURACY REQUIREMENTS VS. SQUINT ANGLE

Azimuth Res (m)	$\Delta \delta_{LOS} (\mu g)$									
	Velocity (ft/sec)									
	760 (450 knots)					912 (540 knots)				
	Squint Angle (°)					Squint Angle (°)				
	20	30	40	50	90	20	30	40	50	90
1	88	188	311	441	752	127	271	447	636	1083
3	792	1692	2797	3972	6769	1140	2437	4027	5720	9747
10	8798	18803	31075	44136	75211	12669	27076	44749	63556	108304
R=30 km=9.84252 x 10 ⁴ ft $\lambda = .106$ ft										

TABLE 6.2 LOS ACCELERATION ACCURACY REQUIREMENTS VS. AIRCRAFT SPEED

Azimuth Res (m)	$\Delta \delta_{LOS} (\mu g)$									
	Velocity (ft/sec)									
	760 (450 knots)			810 (480 knots)			912 (540 knots)			
	Squint Angle (°)			Squint Angle (°)			Squint Angle (°)			
	20	30	90	20	30	90	20	30	90	
1	88	188	752	100	214	854	127	271	1083	
3	792	1692	6769	899	1922	7689	1140	2437	9747	
10	8798	18803	75211	9994	21358	85433	12669	27076	108304	
R=30 km=9.84252 x 10 ⁴ ft $\lambda = .106$ ft										

could adequately motion compensate a SAR with resolution as fine as 3 meters under most

operating conditions. Only during high g aircraft maneuvering and small squint angle operation does the SAR requirement become exceeded by the INS capability. Achieving even finer resolutions than three meters would be possible if imaging was done at ranges shorter than 30 km.

LOS Centripetal Acceleration Error

If the geometry in Figure 6.1 is considered, the velocity accuracy required to limit the LOS centripetal acceleration error to a level consistent with SAR QPE can be determined. The instantaneous aircraft range to the map reference point can be expressed as:

$$R(t) = [R_0^2 + (vt)^2]^{\frac{1}{2}} \quad (ft) \quad (6.6)$$

where R_0 corresponds to the time, $t=0$, at which the aircraft comes closest to the map reference point.

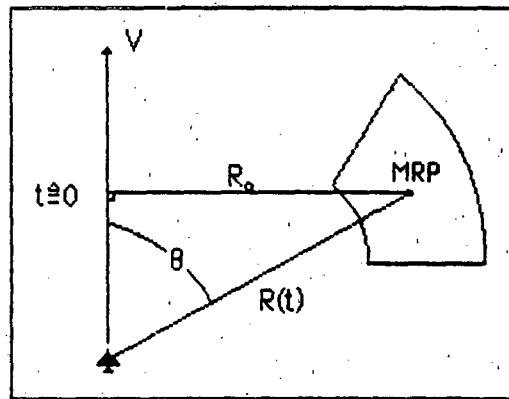


FIG. 6.1 Aircraft Closure Geometry

The corresponding acceleration can be determined as:

$$\dot{R}(t) \cong \frac{\partial R(t)}{\partial t} = \frac{V^2 t}{[R_0^2 + (Vt)^2]^{\frac{1}{2}}} \quad (\text{ft/sec}) \quad (6.7)$$

$$\ddot{R}(t) \cong \frac{\partial^2 R(t)}{\partial t^2} = \frac{V^2 - \dot{R}^2(t)}{R(t)} = \frac{(V \sin \theta)^2}{R(t)} \quad (\text{ft/sec}^2) \quad (6.8)$$

Then the erroneous LOS acceleration due to an error in aircraft velocity is given by:

$$\Delta a_{\text{LOS}} = \frac{\partial \ddot{R}(t)}{\partial V} \Delta V = \frac{2V \Delta V}{R(t)} \quad (\text{ft/sec}^2) \quad (6.9)$$

where the higher order terms have been neglected. Once the relationships for acceleration error, quadratic phase, integration time (Equations 6.9, 6.2, and 2.22) have been combined and imposing the 90 degree QPE criterion yields the desired expression for allowable velocity error:

$$\Delta V = \frac{2V d^2 \sin^2 \theta}{\lambda R} \quad (\text{ft/sec}) \quad (6.10)$$

Velocity accuracy requirements are shown in Table 6.3 and should be compared to the projected aided INS performance capabilities shown in Table 5.2 of roughly one ft/sec. Again it is shown that state-of-the-art INS are capable of providing motion compensation for SAR resolutions as fine as three meters for a wide range of scenarios.

TABLE 6.3 VELOCITY ACCURACY REQUIREMENTS

Azimuth Res (m)	ΔV (ft/sec)								
	Velocity (ft/sec)								
	760 (450 knots)			810 (480 knots)			912 (540 knots)		
	Squint Angle (°)			Squint Angle (°)			Squint Angle (°)		
	20	30	90	20	30	90	20	30	90
1	.18	.39	1.56	.20	.42	1.67	.22	.47	1.88
3	1.65	3.53	14.1	1.76	3.76	15.0	1.98	4.23	16.9
10	18.3	39.2	157	19.6	41.8	167	22.0	47.0	188
R=30 km=9.84252 x 10 ⁴ ft $\lambda = .106$ ft									

VII. Autofocus Techniques

It has been shown that a high degree of compatibility exists between SAR motion compensation requirements and INS performance capabilities but high resolution imaging at long range, small squint angles, low aircraft velocities, and high g maneuvers may impose QPE requirements which cannot be satisfied by aided INS capabilities. In such situations, it may be necessary to perform a post-collection motion compensation correction prior to the Fast Fourier Transform (FFT). It may be noted that normal motion compensation takes place "on-the-fly" as the return data is received by the radar or as a closely associated "one-pass" process. Autofocusing is a technique which extracts information from the partially processed image in order to estimate the residual error phase which is then taken out of the data prior to the full processing. Figure 7.1 illustrates the interface between the autofocus process and the azimuth processing. As can be seen, the two azimuth processing steps are an essential prerequisite for many types of autofocus techniques.

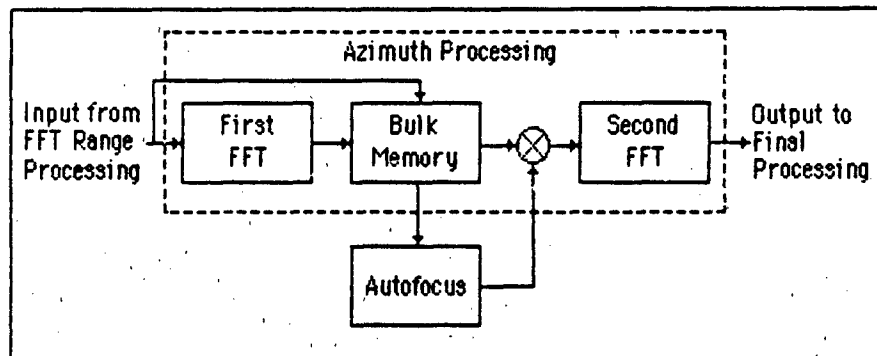


Fig. 7.1 Autofocus Interface (3: 484)

In the last few years, several approaches have been proposed to estimate the amount of QPE present in a radar signal. Some of the earlier methods require certain map structures to

perform successfully, i.e., they require the existence in the map of strong isolated point scatterers. It would be desirable to obtain an autofocus algorithm that performs on any scene structure. An algorithm to accomplish this is called the map drift method of autofocus.

Map Drift Method

The utilization of map drift to measure SAR misfocus dates back to the observation by operators of early SAR systems that focus errors cause azimuth drift of successive maps of the same terrain. This drift is caused by quadratic phase variation in the raw data, which, when integrated over the time difference between two maps of the same scene, results in a linear (with time) phase difference between the data of the two maps. The apparent Doppler shift caused an azimuth offset between the two maps. This source of map drift can be illustrated by Figure 7.2. A quadratic phase variation, assumed zero at the center of the array, is illustrated.

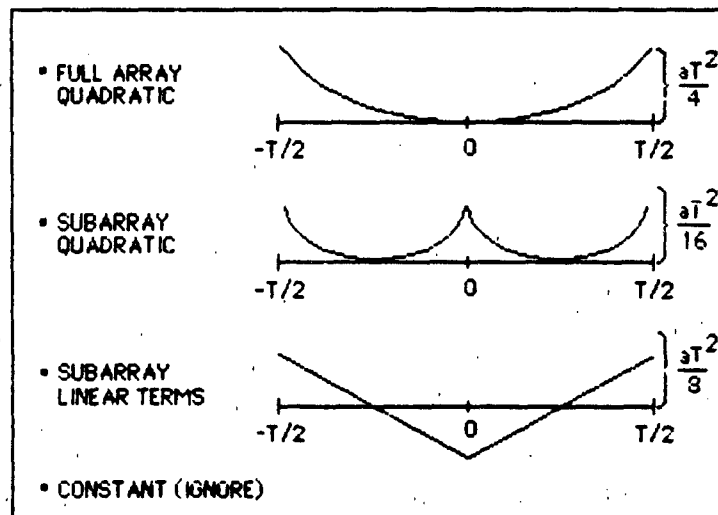


Fig. 7.2 Subarray Linear Phases with Opposite Slopes Caused by Quadratic Phase on Full Array (3: 486)

If the array is divided into two subarrays, the quadratic phase on each side can be considered to

consist of quadratic variation whose maximum value is one fourth that of the full array, in addition to a linear phase term. The difference in the linear phase terms (constant frequency difference) causes the azimuth map offset. The drift between subarray maps can be measured several different ways and each is a candidate for implementation as a quadratic phase estimator. The most obvious method is to cross correlate the subarray maps and choose the lag or offset that maximizes the correlation integral. This approach is outlined in Figure 7.3. The input is a

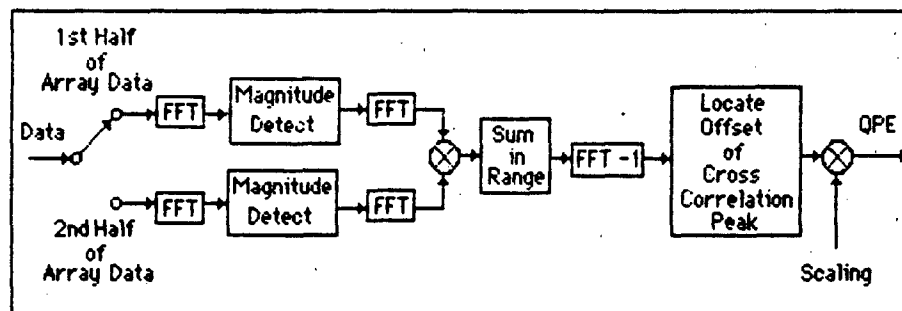


Fig. 7.3 Block Diagram of Map Drift Autofocus Algorithm (16:25)

sequence of data that has been focused approximately by using the best knowledge of the two radar's velocity, acceleration, and antenna look angles. The autofocus algorithm operates on a subarray of data, of width less than 1/2 of the full-resolution array, and forms a map from the magnitudes of the Fourier components after Fourier transformation. The process is repeated later with some nonoverlapping portion of the phase history of the same ground scene, at the same range. The two maps are cross-correlated, and the resulting cross-correlation function is averaged over range to smooth out scintillation and other noise disturbances. The estimated drift in pixels is then taken to be the offset at which the averaged cross correlation function peaks. The accuracy of the offset can be estimated to within less than one pixel by using an interpolating function to find the peak of the sampled cross correlation function. When the subarrays are spaced one-half of the full resolution array length N , the offset in number of pixels on the

subarray map multiplied by π is the estimated residual QPE in radians measured center to end of the full array. Once the QPE has been determined, the full array map data is refocused and then the map is Fast Fourier Transformed and displayed.

SAR Performance Envelopes

As illustrated, the worst case motion compensation conditions indicate difficult requirements on velocity and acceleration motion sensing equipment if sensing and compensation were to be performed in one of the traditional ways. The projected state-of-the-art capability in motion sensing techniques is on the order of 50 to 100 μg acceleration and 0.2 to 0.5 m/sec velocity when considered in terms of operation in a highly maneuverable aircraft. Consequently, a reliance on traditional motion compensation techniques as the only approach to the motion compensation problem would result in degraded performance at the extremes of the operational envelope. Autofocus technology has progressed significantly in the past few years to the point it can be exploited to complement traditional motion compensation approaches to significantly extend the conditions over which desired performance can be achieved. Assessments of SAR have been made on various programs with the conclusion that autofocus techniques are well suited to accommodating large QPE. The upper bound on resolution improvement which can be provided by autofocus is a complex function of clutter-to-noise ratio, scene content, scene size, and higher order phase errors and is just now becoming a topic of both theoretical and experimental investigation. QPE in the region of 24π , 32π , and 40π , have routinely been accurately estimated and compensated in recent programs utilizing high clutter-to-noise ratio data with artificially introduced QPE. These QPE represent nominal values and the maximum achievable QPE compensation has not yet been determined.

To conclude this study, Figure 7.4 illustrates the significance of various levels of motion compensation with and without autofocus. The graphs in this illustration show the range-squint

angle regions where focus can be maintained based on the indicated velocity and acceleration compensation capabilities. The lower set of graphs indicate the performance envelope which can

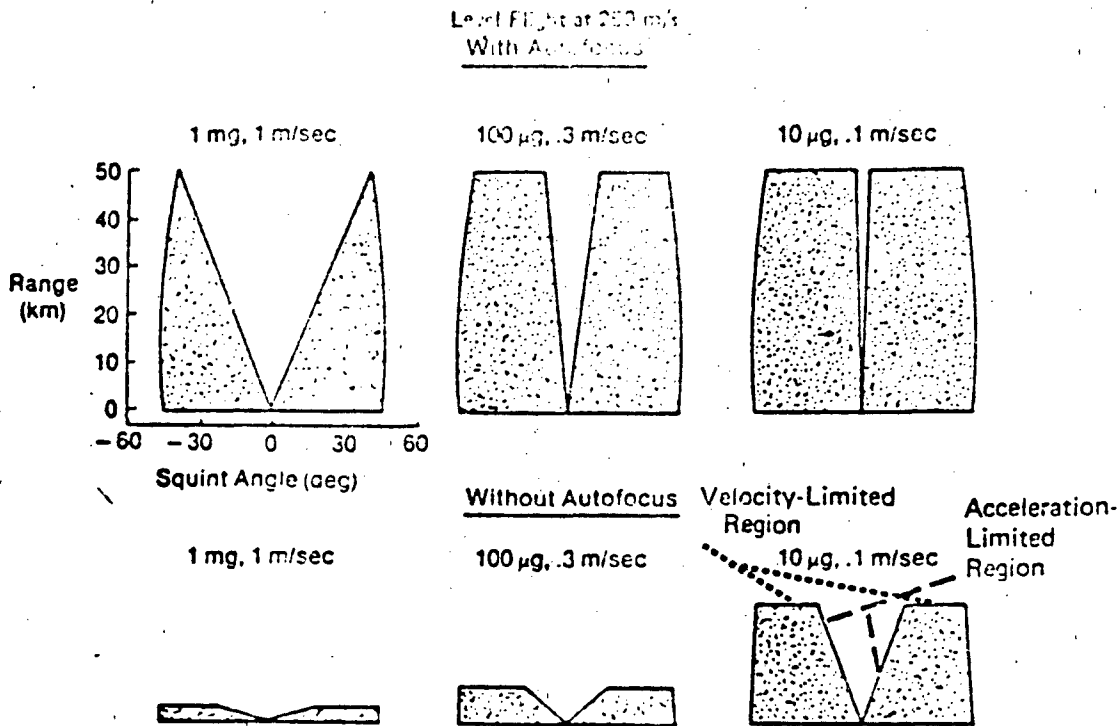


Fig. 7.4 Performance Envelope Sensitivity to Various Levels of Motion Compensation Capability (16:27)

be achieved without autofocus while the above set shows the capability that can be achieved with a 10x improvement via autofocus. The 10x value is a baseline for comparison and was selected to reflect a system mechanization where the inertial motion compensation is designed to accommodate a 10m moderate resolution capability in the first FFT process with a 1m fine resolution capability being provided by a second FFT process. The 10x relates to the fact that the ratio of moderate to fine resolution is 10. This improvement value assumes a QPE reduction of 50π by the autofocus algorithm. The outer squint angle boundaries are determined

by somewhat arbitrary radar waveform ambiguity constraints associated with second time around range echoes and the higher pulse repetition frequencies necessary when imaging at the larger squint angles. Figure 7.4 indicates that the operational envelope is significantly compromised even with a good ($100\mu\text{g}$ and 1 m/sec) motion compensation capability without autofocus. On the other hand, with a 10x autofocus improvement, a very good performance envelope is achievable with what could be termed as a poor (1mg and 3 m/sec) motion sensing capability. Figure 7.5 shows the ability of autofocus augmentation to maintain the range-squint angle performance envelope in the presence of INS acceleration accuracy degradations during aircraft high g maneuvers.

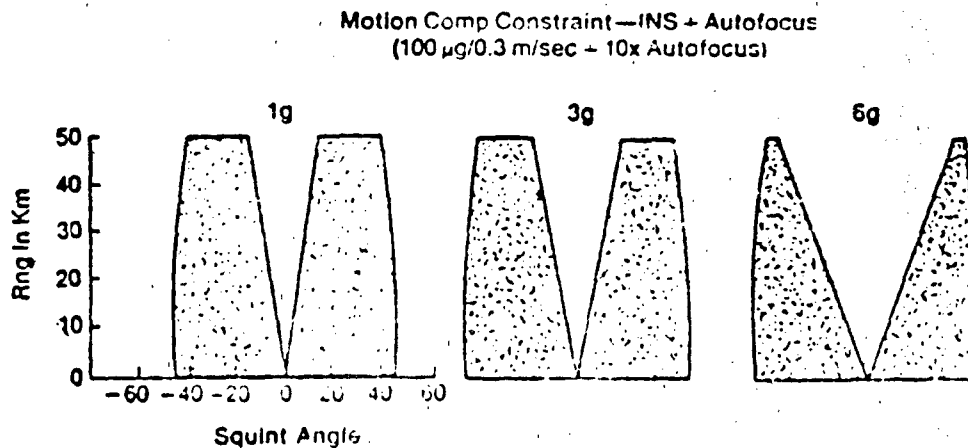


Fig. 7.5 Aircraft Maneuver Effects on SAR Range-Squint Angle Focus Regions

VIII. Conclusions and Recommendations

This study has demonstrated the feasibility of using state-of-the-art strapdown Inertial Navigation Systems to satisfy the motion compensation requirements for Synthetic Aperture Radar onboard maneuvering aircraft. This was accomplished by deriving the equations which related Inertial Navigation System capabilities to Synthetic Aperture Radar motion compensation requirements. Both tuned and ring laser gyro systems were investigated to determine their applicability for the task. In particular, the autofocus technique was discussed for motion compensation. Autofocus is one means of performing the motion compensation function aboard aircraft that are maneuvering as opposed to benign straight and level flight. Autofocus was shown to improve the range and squint-angle boundaries significantly. For a moderate 10x improvement via autofocus, it was shown that the performance envelope for a good (100 μ g and 1 m/sec) motion compensation capability was extended considerably. For a poor (1mg and 3m/sec) motion compensation capability, it was possible with autofocus to have a very useful performance envelope.

The upper bound on resolution improvement which can be provided by autofocus is a complex function of clutter-to-noise, scene content, scene size, and higher order phase errors and should be investigated further to determine the areas in which study should be accelerated. A further investigation into this complex function should be undertaken to determine which areas provide significant improvement in resolution. Also, the outer squint angle boundaries have been determined using arbitrary radar waveform ambiguity constraints and these need to be investigated further to ascertain their appropriateness.

Bibliography

1. Addison, Edwin R. "Alternative Frequency Domain Interpretation Algorithms for Improvement of FFT Outputs in Radar Signal Processing," Proceedings of the IEEE Conference on National Aerospace Electronics (NAECON), 49-53. IEEE Press, New York, 1984.
2. Barton, David K. and Harold R. Ward. Handbook of Radar Measurement. Englewood Cliffs, New Jersey: Prentice-Hall, Inc., 1969.
3. Bendor, G.A. and T.W. Gedra. "Single-Pass Fine-Resolution SAR Autofocus," Proceedings of the IEEE Conference on National Aerospace Electronics (NAECON), 482-488. IEEE Press, New York, May, 1983.
4. Berkowitz, Raymond S. Modern Radar Analysis, Evaluation, and System Design. New York: John Wiley & Sons, Inc., 1965.
5. Blasche, Paul R. Low Frequency Motion Compensation of Synthetic Aperture Radar (SAR) Using the Global Positioning System (GPS). The Charles Stark Draper Laboratory, Inc., Cambridge, Mass., August, 1982.
6. Cutrona, L.J. and G.O. Hall. "A Comparison of Techniques for Achieving Fine Azimuth Resolution," IRE Transactions on Military Electronics, Vol. MIL-6: 119-121 (April 1962).
7. Divakaruni, Dr. Sudhekar P. and Dr. Conrad E. Mueller. "Fast Rection and High Relaiability of Strapdown Navigation Systems Using Ring Laser Gyros," Proceedings of the IEEE Conference on National Aerospace Electronics (NAECON), 315-322. IEEE Press, New York, 1984.
8. Farrell, James L. "Strapdown INS Requirements Imposed by SAR," Proceedings of the IEEE Conference on National Aerospace Electronics (NAECON), 282-288. IEEE Press, New York, 1984.
9. Greene, C. A. and R.T. Moller. "The Effect of Normally Distributed Random Phase Errors on Synthetic Array Gain Patterns," IRE Transactions on Military Electronics, Vol. MIL-6: 130-139 (April 1962).
10. Harger, Robert O. Synthetic Aperture Radar Systems Theory and Design. New York, NY : Academic Press, Inc., 1970.
11. Heimiller, R.C. "Theory and Evaluation of Gain Patterns of Synthetic Arrays," IRE Transactions on Military Electronics, Vol. MIL-6: 122-129 (April 1961).
12. Hovnessian, S.A. Radar Detection and Tracking Systems. Dedham, Mass.: Artech House, Inc., 1973.
13. Hovnessian, S.A. Introduction to Synthetic Array and Imaging Radars. Dedham, Mass.: Artech House, Inc., 1980.

14. Jensen, H., L.C. Graham, L.J. Porcello, and E.N. Leith. "Side-Looking Airborne Radar," Scientific American, Vol. 237, 84-95 (October 1977).
15. Kirk, Jr., John C. "Motion Compensation for Synthetic Aperture Radar," IEEE Transactions on Aerospace and Electronic Systems, Vol. AES-11: 338-348. (May 1975).
16. Kovaly, John J. Synthetic Aperture Radar, Dedham, Mass.: Artech House, 1976.
17. Monem, Sherif A. "Analysis of SAR Azimuth Resolution Using Phasor Approach," Proceedings of the IEEE Conference on National Aerospace Electronics (NAECON), Vol. 1: 296-303. IEEE Press, New York, 1984.
18. Musoff, Howard, George T. Schmidt and George L. McFarland. "Motion-Compensation Requirements for a Synthetic-Aperture Radar (SAR)." The Charles Stark Draper Laboratory, Inc., Cambridge, Massachusetts, 1976.
19. Psota, F. and T. Shenahan. "Gravity Effects on High Accuracy Inertial Navigation," Proceedings of the IEEE Conference on National Aerospace Electronics (NAECON), 310-314. IEEE Press, New York, 1984.
20. Reintjes, J. Francis and Godfrey T. Coate. Principles of Radar (Third Edition). New York: McGraw-Hill Co. Inc., 1952.
21. Ryan, Capt John E. Sensitivity Study of Strapdown Inertial Sensors in High Performance Applications. MS Thesis GE/EE/80D-38. School of Engineering, Air Force Institute of Technology (AU), Wright-Patterson AFB OH, December 1980 (AD-A100825).
22. Siouris, George M. "Investigation of a Strapdown Attitude and Heading Reference System Utilizing Ring Laser Gyros." Proceedings of the Guidance and Control Panel Symposium, 1-13. NATO Advisory Group for Aerospace Research and Development, London, England, 1980.
23. Toomey, J.C. Radar Principles for the Non-Specialist. Belmont, California: Wedsworth, Inc., 1982.
24. Vent, M.R. "A Spatially-Variant Autofocus Technique for Synthetic-Aperture Radar," International Conference RADAR-82, London, UK, 159-163, 18-20 October, 1982.
25. Widhall, William S. and Peter A. Grundy. Inertial Navigation System Error Models. TR-03-73, Intermetrics Inc., Cambridge, Mass., 1973.
26. Wu, K.H. and M.R. Vent. "A SAR Focussing Technique for Imaging Targets With Random Motion," Proceedings of the IEEE Conference on National Aerospace Electronics (NAECON), Vol. 1: 289-295. IEEE Press, New York, 1984.

VITA

Captain Henry D. Baird, Jr. was born on 27 September 1951 in Columbus, Georgia. He graduated from Satellite High School in Satellite Beach, Florida in 1969 and attended Brevard Junior College for one year before entering the United States Marine Corps. Upon honorable discharge from the Marine Corps, he returned to Brevard Community College and received his Associate of Arts degree in 1974. He transferred to the University of Florida and graduated in December 1976 with the degree of Bachelor of Science in Mechanical Engineering. Upon graduation, he received a commission in the USAF through the ROTC program. He completed navigator training and received his wings in December 1976. He then served as a Weapon Systems Officer and Instructor Weapon Systems Officer in the F-111A/E/D in the Tactical Air Command and US Air Forces Europe until entering the School of Engineering, Air Force Institute of Technology, in May 1983.

Permanent address: 716 S. Gardenia Dr.

Melbourne, FL 32901

UNCLASSIFIED

SECURITY CLASSIFICATION OF THIS PAGE

REPORT DOCUMENTATION PAGE

1a. REPORT SECURITY CLASSIFICATION UNCLASSIFIED		1b. RESTRICTIVE MARKINGS	
2a. SECURITY CLASSIFICATION AUTHORITY		3. DISTRIBUTION/AVAILABILITY OF REPORT	
2b. DECLASSIFICATION/DOWNGRADING SCHEDULE		Approved for public release; distribution unlimited.	
4. PERFORMING ORGANIZATION REPORT NUMBER(S) AFIT/GA/ENG/84D-1		5. MONITORING ORGANIZATION REPORT NUMBER(S)	
6a. NAME OF PERFORMING ORGANIZATION School of Engineering	6b. OFFICE SYMBOL (If applicable) AFIT/EN	7a. NAME OF MONITORING ORGANIZATION	
6c. ADDRESS (City, State and ZIP Code) Air Force Institute of Technology Wright-Patterson AFB, OH 45433		7b. ADDRESS (City, State and ZIP Code)	
8a. NAME OF FUNDING/SPONSORING ORGANIZATION Aeronautical Systems Division	8b. OFFICE SYMBOL (If applicable) ENSSC	9. PROCUREMENT INSTRUMENT IDENTIFICATION NUMBER	
8c. ADDRESS (City, State and ZIP Code) Wright-Patterson AFB, OH 45433		10. SOURCE OF FUNDING NOS.	
11. TITLE (Include Security Classification) See Box 19		PROGRAM ELEMENT NO.	PROJECT NO.
12. PERSONAL AUTHOR(S) Henry D. Baird, Jr., B.S., Captain, USAF		TASK NO.	WORK UNIT NO.
13a. TYPE OF REPORT MS Thesis	13b. TIME COVERED FROM _____ TO _____	14. DATE OF REPORT (Yr., Mo., Day) 1984 December	15. PAGE COUNT 56
16. SUPPLEMENTARY NOTATION			
17. COSATI CODES		18. SUBJECT TERMS (Continue on reverse if necessary and identify by block number)	
FIELD	GROUP	Autofocus Motion Compensation ,	
17	09	Synthetic Aperture Radar, ,	
		Strapdown Inertial Navigation .	
19. ABSTRACT (Continue on reverse if necessary and identify by block number)			
Title: AUTOFOCUS MOTION COMPENSATION FOR SYNTHETIC APERTURE RADAR AND ITS COMPATIBILITY WITH STRAPDOWN INERTIAL NAVIGATION SENSORS ON HIGHLY MANEUVERABLE AIRCRAFT			
Thesis Chairman: Dr. George M. Siouris			
20. DISTRIBUTION/AVAILABILITY OF ABSTRACT UNCLASSIFIED/UNLIMITED <input checked="" type="checkbox"/> SAME AS RPT. <input type="checkbox"/> DTIC USERS <input type="checkbox"/>		21. ABSTRACT SECURITY CLASSIFICATION UNCLASSIFIED	
22a. NAME OF RESPONSIBLE INDIVIDUAL Dr. George M. Siouris Lecturer in Electrical Engineering		22b. TELEPHONE NUMBER (Include Area Code) 513-476-0056	22c. OFFICE SYMBOL ENSSC

This study investigated the feasibility of using state-of-the-art strapdown inertial navigation systems to motion compensate synthetic aperture radar aboard highly maneuverable aircraft. The applicable equations were first derived to obtain a comparison between inertial navigation system capabilities and synthetic aperture radar motion compensation requirements. Both tuned gyro and laser gyro systems were investigated to determine the applicability for the task. The autofocus motion compensation technique was studied to determine if its range and squint angle boundaries could be improved by the use of highly accurate strapdown inertial navigation system measurements.

It was determined that state-of-the-art strapdown inertial systems have the capability to motion compensate synthetic aperture radars in maneuvering aircraft and in fact can improve the range and squint angle boundaries using the autofocus motion compensation technique. The results illustrate the ability of tactical aircraft to obtain high resolution imagery, as well as navigation and target information, while maintaining the low life-cycle cost of the strapdown technology. Further study is warranted to simulate via computer the combination of strapdown inertial navigation system and synthetic aperture radar.

END

FILMED

4-85

DTIC